Size Distribution of Coastal Aerosols: Effects of Local Sources and Sinks

K. KRISHNA MOORTHY, PRABHA R. NAIR AND B. V. KRISHNA MURTHY

Space Physics Laboratory, Vikram Sarabhai Space Centre, Trivandrum, India

(Manuscript received 7 May 1990, in final form 2 December 1990)

ABSTRACT

Using aerosol optical depth as a function of wavelength obtained from ground-based multiwavelength radiometer observations, columnar size-distribution functions of aerosols have been derived. It has been found that the nature of the derived size-distribution function is strongly dependent on season. The derived size-distribution functions are discussed in terms of seasonally dependent natural aerosol sources and sinks.

1. Introduction

In studies of radiative transfer in the terrestrial atmosphere and on remote sensing in the visible and infrared wavelengths using spaceborne platforms, one of the most important aspects to be considered is the interaction of electromagnetic radiation with atmospheric aerosols. The scattering and absorption caused by aerosols are strongly dependent on the ratio of the aerosol size to the wavelength of the radiation (particle size parameter), and also the refractive index. Produced by a variety of natural and anthropogenic processes, the aerosols are polydisperse with sizes extending from 10^{-3} to 10^{2} μm (Junge 1963; Prospero et al. 1983). During their lifetime in the atmosphere, the size distribution is modified by various physical and chemical processes. In order to understand the effects of aerosols on radiation, it is essential to characterize the size distribution. Many studies have been carried out on the size distribution of aerosols using both in situ and remote sensing methods (Box and Lo 1976; De Luisi et al. 1976; King et al. 1978).

Spectral optical depths due to atmospheric aerosols estimated from measurements of directly transmitted solar flux in the visible and near infrared, using ground-based solar radiometers, have been used for deducing the height-integrated (columnar) size distribution functions of large and giant aerosols with radii in the range ~0.1 to ~5 μm (Quenzel 1970; Shaw et al. 1973; King et al. 1978; Box et al. 1981). This indeed is the size range relevant in radiative transfer studies involving solar radiation. In this paper we present size-distribution functions obtained from aerosol optical depth measurements at eight narrow spectral bands made over a period of three years using a ground-based solar radiometer at a coastal station. The observed features are examined for the effects of natural sources and sinks that are of a seasonal nature. The implications of the findings are discussed.

2. Aerosol spectral optical depths

Aerosol columnar optical depths have been estimated at nine narrow spectral bands centered at 400, 450, 500, 590, 700, 750, 800, 935 and 1025 nm using a ground-based multiwavelength solar radiometer at the tropical coastal station Trivandrum (8.55°N, 77°E) situated at the southwest coast of India. The instrument, details of which are given elsewhere (Moorthy et al. 1989), is similar in design and operation to the conventional filter-wheel radiometers (Shaw et al. 1973). The bandwidth (full width at half maximum) of each of the interference filters is 5 nm and the overall field of view of the system is less than 2°. A UDT 455 photo detector device serves as the detector. Using this system, spectral measurements of ground reaching solar flux have been made for about 160 days during the period November 1985–December 1988, when the sky was apparently clear and cloud free. Optical depths τ at each spectral band have been computed following the "Langley plot" method from which the contributions due to Rayleigh scattering τ_R and absorption by ozone τ_{O_3} were removed; using relevant altitude profiles of neutral atmosphere and ozone for Trivandrum and the appropriate wavelength dependent cross sections for molecular scattering and absorption by ozone (Moorthy et al. 1989). Optical depth at 935 nm in conjunction with that at 800 and 1025 nm has been used to estimate the columnar content of atmospheric water vapor W. The selective and nonselective absorption due to water vapor τ_W at the other wavelengths is obtained using W and the relevant cross sections (Leckner 1978; Tomasi 1979). The optical depths at

Corresponding author address: Dr. B. V. Krishna Murthy, SPL, Vikram Sarabhai Space Center, Trivandrum 695 022, India.

all the wavelengths are then corrected for τ_W to obtain the optical depths due to aerosols τ_p.

3. Size distributions

Using aerosol optical depths at the eight wavelengths (excluding 935 nm) the columnar (height integrated) size-distribution functions of aerosols have been determined by numerical inversion of the integral equation

$$\tau_p(\lambda) = \int_{r_a}^{r_b} \pi r^2 Q_{\text{ext}}(r, \lambda, m) n_c(r) dr \qquad (1)$$

where r is the particle radius; r_a and r_b are the inner and outer radii limits, respectively; Q_{ext} is the Mie extinction efficiency parameter; and m is the refractive index of aerosols. The quantity $n_c(r)dr$ is the columnar size distribution of aerosols given by

$$n_c(r)dr = \int_0^{\infty} n(r)drdh \qquad (2)$$

where $n(r)dr$ is the number of particles in unit volume of atmosphere in a size range dr centered at r. The wavelength 935 nm was primarily meant for estimation of columnar content of atmospheric water vapor. As this wavelength lies close to the peak of the $\rho\sigma\tau$ band of water vapor, about 75%–90% of the measured optical depth at this wavelength is due to atmospheric water vapor, depending on its content. Thus, any small error in the estimate of W could result in a significant error in τ_p at 935 nm. However, at other wavelengths the absorption cross section of water vapor is more than two orders smaller (e.g., Leckner 1978) and as such, the errors introduced in τ_p by uncertainties in W estimated from τ at 935 nm will not be significant. Because of this reason τ_p at wavelength 935 nm is not included in the inversion of the size distribution, particularly in the light of the known sensitivity of the inversion technique to errors in the measurements.

The inverse problem of obtaining the indicial function $n_c(r)dr$ from the measurements of τ_p and a fairly known form of the kernel function is quite complex due to instability of the solutions (Phillips 1962; Twomey 1963). This instability is mainly the consequence of errors in the measurements of $\tau_p(\lambda)$, and those arising due to the departure of the assumed kernel function from the true function. Thus, in order to obtain physically meaningful solutions from a family of possible solutions, constraints have to be applied. The relative advantages of such constrained linear inversion of the integral equation, making use of a Lagrange multiplier, have been described in detail in the literature (e.g., King et al. 1978; King 1982) and as such this aspect will not be dealt with here. In the present work the solutions have been obtained following the iterative inversion method described by King (1982), assuming an inverse power-law form for the zero-order function. The constraints used are (i) that the solution vectors should all be positive (ii) that the Lagrange multiplier (which should be positive) is varied each time and the lowest value is selected when all the solution vectors become positive for the first time, and (iii) that the optical depths reestimated using the solution size distributions should match the measurements within experimental errors. For data on individual days the experimental errors correspond to the measurement errors arising from (a) the instrumentation and (b) estimation of τ_p from measurements. The final error bars are calculated knowing the individual errors and using the principle of propagation of errors (Ku 1966; Meyer 1975) for independent errors. However, when individual data are averaged on a monthly basis, the standard error of the mean τ_p at each wavelength also has been considered along with the measurement errors. While applying the last constraint mentioned above in deducing the size distributions, it was ensured that the sum of errors in the reestimated τ_p at all the wavelengths is less than the sum of measurement errors in τ_p; and also at any single wavelength the difference between the reestimated and measured values of τ_p did not exceed twice the error at that wavelength. In general the number of iterative steps in obtaining the size distributions did not exceed 6–8. Three sets of values have been tried for r_a and r_b in the range 0.05–10 μm, and the range 0.1–5 μm has been found to be the optimal. As coastal aerosols are hygroscopic it is reasonable to assume that their refractive index is wavelength dependent. We have adopted the wavelength-dependent refractive index values as given by Shettle and Fenn (1979) in the present investigation. King et al. (1978) studied the effect of changes in refractive index values on the inverted size distributions and found that the shape of the inverted size distribution is not affected significantly by changes in refractive index. The size distributions have been estimated as described above and are plotted on a log–log scale. Total columnar content of aerosols N_t in the size range 0.1–5 μm has been evaluated by integrating $n_c(r)dr$ so that

$$N_t = \int_{r_a}^{r_b} n_c(r)dr. \qquad (3)$$

A sample size-distribution function, which is obtained for the data on 13 April 1988, is shown in Fig. 1, where the vertical bars correspond to the standard deviations of the solution points that are obtained as the square root of the diagonal elements of the solution covariance matrix (King 1982). The top panel of the same figure shows the measured $\tau_p(\lambda)$ values at different wavelengths (as points with error bars) along with the τ_p values reestimated using the solution size distributions in Eq. (1) (shown by continuous line). Size distributions, thus obtained for the entire data, have then been examined for various features.

Fouquart et al. (1984) compared the size distribution

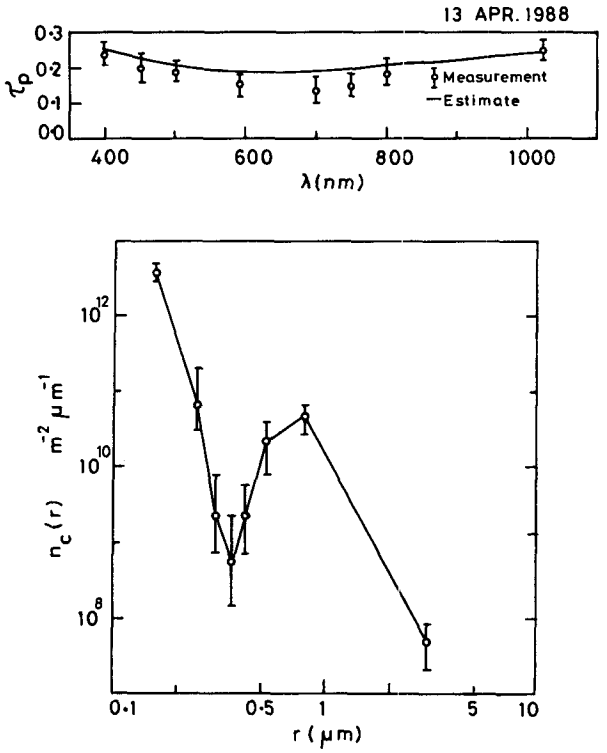

FIG. 1. Size-distribution function of aerosols obtained for optical depth data on 13 April 1988 showing a bimodal nature.

obtained from inversion of spectral optical depth measurements (as in the present investigation) with that obtained from cascade impactor and found good agreement between the two, especially in its nature of variation with size. So while there may be some uncertainty regarding the true number density values in the size distributions obtained by inversion of the spectral optical depth measurements, the functional form obtained can be taken to represent the actual one, as far as the optical effects are concerned. Thus, it is to be noted that the following discussions on size distributions obtained from inversion of spectral optical depths pertain mainly to their functional form than to their quantitative feature like number density at a given size.

4. Results

a. General features

An examination of the individual size distributions revealed that they can broadly be classified into three groups depending on their shape; viz., the modified Junge type (MJ), the unimodal (UM), and the bimodal (BM) distributions. The MJ distribution is characterized by a nearly flat region at lower particle sizes with the number density decreasing slowly with increase in particle radius, then a break around 0.3 μm followed by a nearly monotonic decrease (nearly linear on a log–log scale). An example of such distribution is shown in Fig. 2, which has been obtained for the optical depth data of 29 January 1987. The UM type shows a pronounced mode at some value of the radius with the aerosol content falling off on either side of the mode. An example of this distribution is shown in Fig. 3, which is obtained for 14 October 1988. The third type (BM) is characterized by a secondary mode occurring at a fairly large value of r while the primary mode does not appear explicitly (perhaps occurring at or below $r = 0.1$ μm). This type of distribution resembles the one shown in Fig. 1. All the observed distributions broadly fall under one of the above three types, according to their shape, even though other characteristics such as the mode radii and the total columnar content N_t could be different.

The wavelength variation of τ_p shown in the top panels of Figs. 1–3 is characteristic of the particular type of distribution appearing below. The characteristic feature is that the spectral variations of τ_p appear somewhat similar when the aerosol-size distributions are MJ and UM but are distinctly different when the distribution is BM. In the former cases, τ_p either remains constant or initially shows an increase with increase in wavelength at short wavelength end, reaching a peak value in the range 450–590 nm. At the peak,

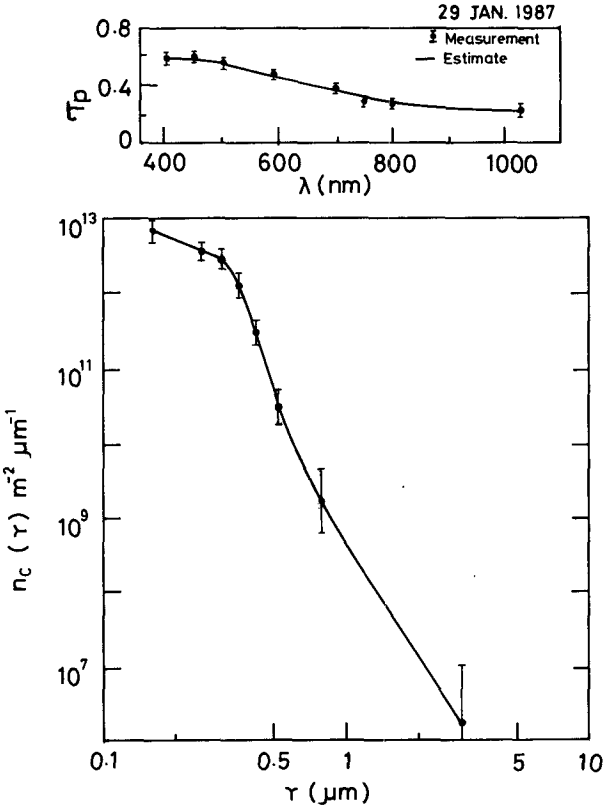

FIG. 2. Typical MJ size distribution obtained using data on 29 January 1987.

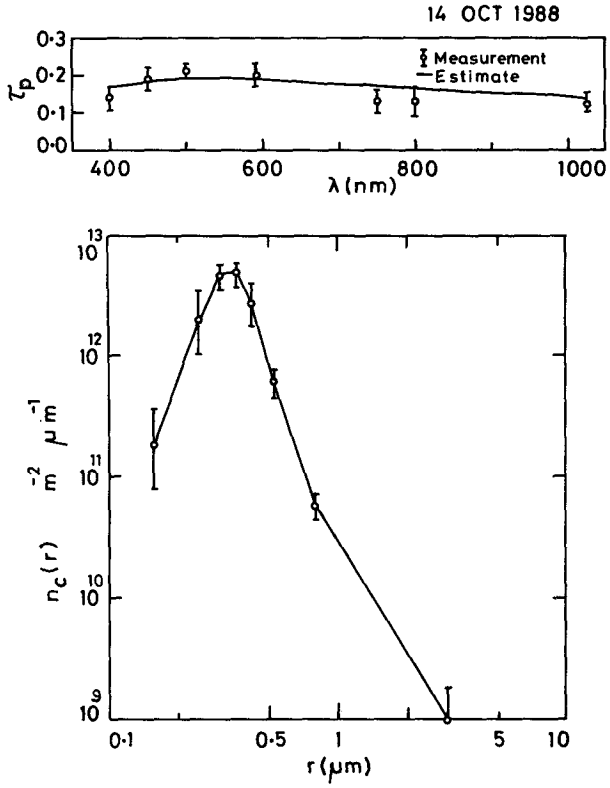

FIG. 3. Typical UM distribution obtained using data on 14 October 1988.

the variation shows a negative curvature leading to a gradual decrease in τ_p at longer wavelengths. When the distribution is bimodal, an opposite behavior is seen; τ_p continuously decreases with increase in wavelength and then shows a gradual increase, though small, at longer wavelengths—the curve showing a positive curvature in the range 700–800 nm.

b. Seasonal changes

A survey of the individual τ_p–λ plots showed a seasonal pattern in their behavior. This aspect has been studied in detail by obtaining representative size distributions for every month. This has been done by averaging the daily τ_p values at each wavelength on a monthly basis and inverting the average τ_p–λ values. In this case, the standard error of the mean over and above the individual error is included in the measurement error as described earlier. The number of days in a month varied from 5 to 10. But during June–September, which are months of intense monsoon (southwest) activity, the data is in general, scarce due to adverse sky conditions. Figures 4 and 5 depict typical distributions obtained during the local summer months (March–May) and northeast monsoon and winter months (October–February), respectively. The summer distributions are generally bimodal (BM) while the winter ones are unimodal (UM). In the southwest monsoon months (June–September) both types of distributions (BM and UM) occur. In Table 1 a summary of the distributions for the entire data is given. The mode radius was obtained as the radius corresponding to the peak in the distribution, and the columnar content by integrating the distribution function (numerically) as given by Eq. (3).

It is seen from Table 1 that during northeast monsoon and winter months (October–February) the distribution is unimodal, in general. Out of a total of 15 months of northeast monsoon and winter for which data have been analyzed, 11 months showed UM distribution; the average value of the mode radius being 0.35 ± 0.06 μm. During summer and monsoon (southwest) months the distributions are, in general, BM (7 out of 10), with the second mode in the range of 0.6–0.8 μm.

A perusal of Table 1 reveals that the total aerosol content, generally, is very low in the year 1988 compared to the previous two years. In particular, it is lower during the period November 1987–October 1988, compared to same periods in other years (January and February months of 1986 are exceptions). However, the seasonal patterns are similar in these years. With

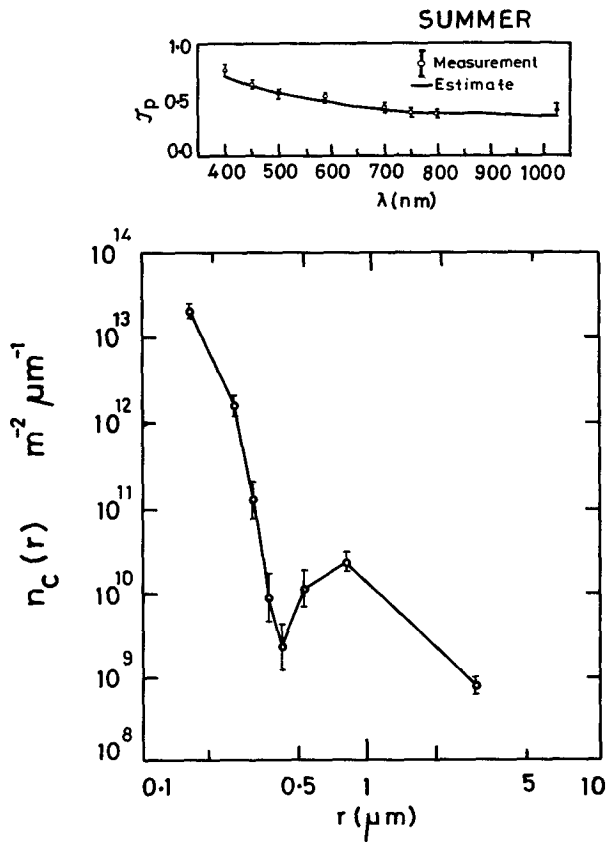

FIG. 4. Aerosol-size distribution during summer months.

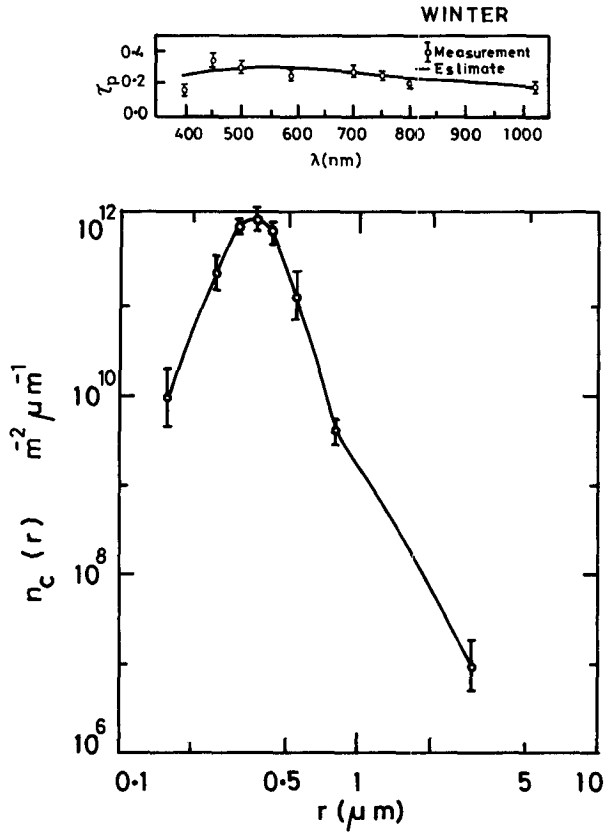

FIG. 5. Aerosol-size distribution during winter months.

a view to examining this further, we have shown in Fig. 6, the weighted mean radius R of aerosols as a function of month. Here, R is given by

$$R = \frac{\int_{r_a}^{r_b} n_c(r) r dr}{\int_{r_a}^{r_b} n_c(r) dr} \qquad (4)$$

and represents the radius about which the total columnar content is distributed equally in the range r_a to r_b, such that columnar content in the range r_a to R is equal to that in the range R to r_b. Also shown in the figure is the aerosol content below and above $r = 0.42$ μm and monthly total rainfall recorded at Trivandrum. The radius of 0.42 μm is taken to demarcate large and small particles.

Figure 6 reveals certain distinct features for the year 1988 (in fact from November 1987 to October 1988) compared to the previous two years; (a) the weighted mean radius R is in general greater; (b) the total content of large particles with $r > 0.42$ μm is, in general, higher; and (c) the total content of small particles with $r < 0.42$ μm is in general, significantly lower. The month September 1988, however, is an exception and does not fall in line with the general pattern. An examination of the monthly rainfall data shown on top panel of Fig. 6 clearly reveals that during 1987, the rainfall during the northeast monsoon months (October–December) has been extraordinarily high (amounting to ~53% of the total rainfall) compared to the other years. As seen from Table 2, which gives the rainfall (recorded at Trivandrum) during the two monsoons and the total rainfall for the years 1986, 1987, and 1988, the northeast monsoon rainfall in 1987 was about 6–7 times higher compared to that in the other two years, whereas the southwest monsoon rainfall was lower in 1987 compared to that in the other two years. Thus it appears that the abnormally heavy rainfall during northeast monsoon months of 1987 removed lower tropospheric aerosols substantially by wet scavenging. The consistently low values of total aerosol loading (Table 1) in 1988 indicate that the wet scavenging has been very effective and the subsequent build up did not replenish the loss entirely. It also appears from Fig. 6 that the build up of large particles with $r > 0.42$ μm is faster compared to that of small particle ($r < 0.42$ μm) concentration. This could be attributed to the distinct production mechanisms of the large and small particles. The small particles are generally produced by gas-to-particle conversion processes and subsequent coagulation and nucleation, while large particles are mostly mechanically generated by bulk-to-particle conversion such as sea spray or land-blown dust (Prospero et al. 1983; Jaenicke 1984).

5. Discussion

Study of the aerosol-size distribution deduced from spectral optical depth data for 25 months spread over a 3-yr period shows that most of the time the distributions exhibit modal structure. Mainly they fall under two groups, namely, the unimodal and bimodal. The unimodal (UM) shows a single pronounced mode at a radius in the range 0.3–0.4 μm. In the bimodal (BM) distribution while the primary mode is not apparent, the secondary mode occurs in the range 0.6–0.8 μm. The spectral variation of aerosol optical depth associated with UM distribution shows a negative curvature with an initial increase in τ_p followed by a gradual decrease, whereas, that associated with the BM distribution shows a positive curvature. Analyzing solar extinction data obtained over Tucson, King et al. (1978) have reported a similar association between optical depths and size distributions.

As far as seasonal changes in the size-distribution function are concerned, the observations reveal that the inverted distributions are, in general, unimodal during October–February (barring a few cases), while during March through September the distribution is mostly bimodal. This seasonal pattern is generally repeated over the three years. As the station Trivandrum is free from any major industrial effluevia, the expla-

TABLE 1.

Year	Distribution	Premonsoon summer			Southwest monsoon				Northeast monsoon and winter				
		Mar	Apr	May	Jun	Jul	Aug	Sep	Oct	Nov	Dec	Jan	Feb
1985–86	Type									MJ	UM	UM	MJ
	r_m									0.38	0.38	0.38	0.31
	N_t									0.46	0.46	0.10	0.16
1986–87	Type			BM					BM		UM	UM	BM
	r_m			<0.1; 0.65					<0.1; 0.65		0.31	0.32	<0.1; 0.67
	N_t			1.9					0.85		0.30	1.3	1.1
1987–88	Type	BM	BM					BM		UM	UM	UM	UM
	r_m	<0.1; 0.8	<0.1; 0.8					<0.1; 0.8		0.48	0.37	0.28	0.30
	N_t	2.5	1.9					0.54		0.04	0.17	0.32	0.25
1988	Type	UM	BM	UM	BM	UM		BM	UM	UM	UM		
	r_m	0.36	<0.1; 0.75	0.36	<0.1; 0.6	0.43		<0.1; 0.65	0.40	0.37	0.30		
	N_t	0.14	0.35	0.26	0.06	0.10		0.41	0.11	0.17	0.55		

MJ: modified Junge; UM: unimodal; BM: bimodal; r_m: mode radius (μm); N_t: columnar content (10^{12} m^{-2}).

nation for the observed seasonal changes in the shape of the deduced size-distribution functions should be sought in terms of natural sources and/or sinks of aerosols. In this context the parameters of importance are the monsoon rains and the associated changes in the boundary-layer wind system that show a distinct seasonal pattern. Typically, southwest monsoon sets in at Trivandrum in the first week of June and lasts till the end of September. This period is characterized by extensive rainfall and strong west-southwesterly surface winds that blow from the sea towards land (Rao 1976). Another spell of rainfall occurs during October–December which is the northeast monsoon. During this period (known as the return monsoon) the circulation is mostly northeasterly in nature in the upper boundary layer even though the surface winds near the coast continue to be westerly, but weak. The monthly distribution of average rainfall is shown in Fig. 6 for the period November 1985–December 1988. The monthly average westerly wind recorded at Trivandrum, about 500 m off the coast and about 3 m above the surface during the above months is shown in Fig. 7. Due to the proximity to the coast a westerly wind always prevails at the station during most of the daytime owing to the sea breeze. However, from the end of March onward, a strong westerly component is added to this arising from the premonsoon (southwest) surface westerlies as evidenced by the sharp increase in the average wind around March–April (Fig. 7). This effect continues till the end of September which also marks the end of the main monsoon activity. These strong surface westerlies lead to agitation of the sea surface resulting in surf and white caps. A considerable amount of marine aerosols is produced due to sea surf whose size spectrum and abundance depends on the wind speed (Junge 1963). These marine aerosols are brought over to the coastal land area by the westerlies. Such observations of marine aerosols transported over to coastal land by wind have also been reported by Suzuki and Tsunogai (1988) at a coastal station in Japan. These sea-spray particles are also known to be fairly large with sizes typically >0.3 μm (Junge 1963). These aerosols add to the already existing background to produce a secondary mode at a large particle size leading to bimodal distributions in the premonsoon summer months. Other processes of generation of aerosols, like the action of wind on rather dry land and those of vegetative origin could also be important. The wet removal processes are not active during premonsoon periods as the total average rainfall during January–May has only been 15% of the annual, during the period of study.

Significant wet scavenging of lower-tropospheric aerosols by the strong monsoon rains dominates the southwest monsoon months, which extend from June until the end of September. The production of sea-spray aerosols by the action of surface westerlies also is strong, being strongest in July when the wind speeds

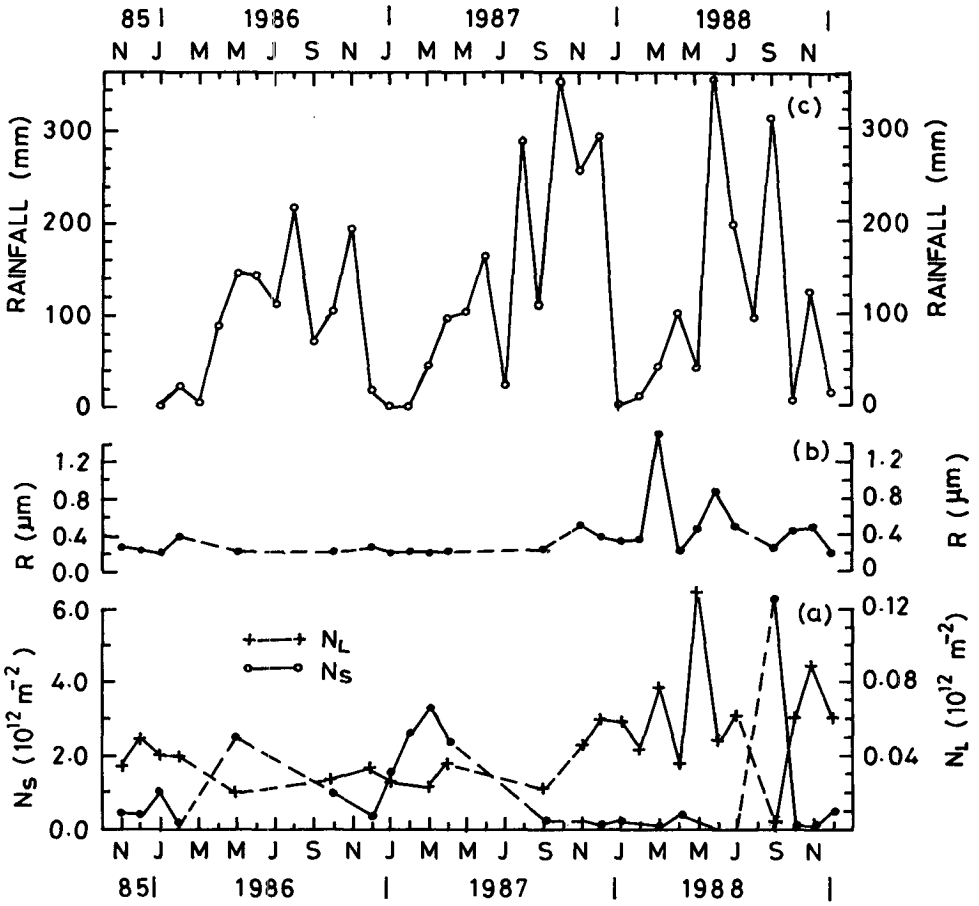

FIG. 6. Variation of (a) aerosol content for $r < 0.42$ μm (points marked as dots and scale on lhs) and for $r > 0.42$ μm (points marked with crosses and scale on rhs), (b) weighted mean radius R, and (c) monthly total rainfall. Dashed lines correspond to absence of data.

are highest. Model calculations by Flossmann et al. (1985) and Flossmann and Pruppacher (1988) for chemically homogenous particles reveal that wet scavenging (combined effects of nucleation and impaction scavenging) can reduce the number concentration of aerosols by 48% to 94% depending on their composition. They have also shown that this effect is confined mainly to particles with radius > 0.1 μm. These two competing processes, namely, sea-spray aerosol production, and wet scavenging, influence the size distribution depending on their relative dominance. This may result in BM or UM distribution depending on which process is dominant, as seen in the months of July and September.

TABLE 2.

Year	Amount of rainfall (mm)		
	Annual	Southwest monsoon (June–September)	Northeast monsoon (October–December)
1986	1144	846	118
1987	1728	563	916
1988	1291	956	142

The monsoon associated westerlies become weak by the end of September as the southwest monsoon activity withdraws. The average wind in October is about half in magnitude of that during the southwest monsoon season as seen from Fig. 7. The sea surface becomes relatively calm. The rainfall during the months of October–December is considerable, thereby effecting wet scavenging. The production of marine aerosols by sea spray is very weak with the consequence of the disappearance of the secondary mode in the inverted distributions by October. Thereafter, the distribution continues to be unimodal till the next premonsoon season. The total loading is now determined by the competing actions of wet scavenging and transport of continental aerosols.

Aerosol extinction profiles obtained by lidar experiment at Trivandrum (Parameswaran et al. 1989) show that nearly 90% of the total aerosol extinction is contributed by the first 8 km and about 20% by the first

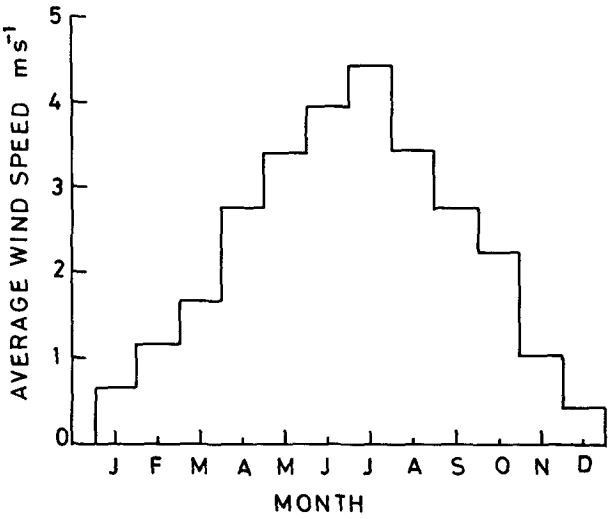

FIG. 7. Monthly distribution of average speed of westerly wind for the period November 1985–December 1988.

1-km region of the atmosphere above ground. Thus the aerosol optical depth measurements in the present investigation can be attributed mostly to the height range from 0 to 8 km (integrated).

Typical size distributions of coastal aerosols include both continental (large concentration of small particles) and maritime (large particles) components (Prodi et al. 1983) and thus will be bimodal in shape (Hoppel et al. 1985). The dominance of the large particle mode depends upon the extent of contribution of the maritime component. At Trivandrum, it is observed that the derived size distributions are bimodal, in general during summer and monsoon (southwest) season when the maritime component is strong. During northeast monsoon and winter months of October to February, the distributions are, in general, unimodal with a mode radius of $\sim$0.35 μm. In the size range under consideration basically two aerosol production mechanisms are operative. These are gas-to-particle conversion and bulk-to-particle conversion (Jaenicke 1984). The former process is effective mainly for the submicron sizes whereas the latter is effective for the larger sizes. The bulk-to-particle conversion includes processes such as weathering, raising dust and sea-salt spray. These can be considered not to be significant in the northeast monsoon and winter months at Trivandrum. The gas-to-particle conversion process involves condensation of vapors (either by homogeneous or by heterogeneous condensation) preceded in many cases by gaseous chemical reactions that are generally initiated by photochemical processes (Mészáros 1981; Whitby 1978). These processes are expected to be weaker in the winter season (Mészáros 1981). Thus the size distributions obtained in the present investigation during October through February (northeast monsoon and winter months) can essentially be considered to correspond to aging (or background) aerosols in the absence of strong production mechanisms. Particles with sizes around 0.3 μm have the longest residence times compared to the smaller and larger sizes (Jaenicke 1984). Smaller particles are affected by coagulation processes and the larger particles by sedimentation processes. Thus the unimodal size distributions in the northeast monsoon and winter season are consistent with the above considerations.

In addition to the above-discussed processes associated with seasonal sources and sinks, the changes in relative humidity RH at the lower atmosphere also could play a role in modifying the size distribution. The measurement of surface RH over Trivandrum shows that it is maximum during monsoon months (Parameswaran and Krishna Murthy 1990). Since the coastal aerosols are likely to be hygroscopic in nature, condensation growth of particles can occur during periods of high relative humidity. Computations by Hänel (1976), and by Shettle and Fenn (1979) for typical aerosol models show the effect of RH on growth of particles leading to increase in the mode radii. This could be true with the present observations too. The shift in the mode radius from 0.35 μm during winter periods to 0.43 μm in July (peak monsoon) could be at least partly attributed to this effect. However, the condensation growth cannot explain the appearance of the secondary mode in the range 0.6 μm, which is more than double the mode radius during winter.

6. Conclusions

The radiometer observations made at the coastal station Trivandrum, India have revealed that

(i) The columnar size-distribution function of aerosols derived by inversion of the spectral optical depths, in general, shows either a UM pattern or BM pattern.

(ii) The data over three years show that the size distributions are, in general, unimodal in the northeast monsoon and winter months. The mode radius generally varies from 0.30 to 0.4 μm with a mean value of $\sim$0.35 μm. The distributions are mostly bimodal in summer and southwest monsoon months.

(iii) Wet scavenging leads to a significant drop in aerosol loading and consequently to depleted optical depths.

REFERENCES

Box, G. P., M. A. Box and A. Deepak, 1981: On the spectral sensitivity of the approximate method for retrieving aerosol size distributions from multispectral solar extinction measurements. *J. Appl. Meteor.*, **20**, 944–948.

Box, M. A., and S. Y. Lo, 1976: Approximate determination of aerosol size distributions. *J. Appl. Meteor.*, **15**, 1068–1076.

DeLuisi, J. J., P. M. Farukawa, D. A. Gillette, B. G. Schuster, R. J. Charlson, W. M. Porch, R. W. Fegley, B. M. Herman, R. A. Rabinoff, J. T. Twitty and J. A. Weinman, 1976: Results of a

comprehensive atmospheric aerosol radiation experiment in the southwestern United States—Part I: Size distribution, extinction optical depth, and vertical profiles of aerosols suspended in the atmosphere. *J. Appl. Meteor.*, **15,** 441–463.

Flossmann, A. I., W. D. Hall and H. R. Pruppacher, 1985: A theoretical study of the wet removal of atmospheric pollutants—Part I: The redistribution of aerosol particles captured through nucleation and impaction scavenging by growing cloud drops. *J. Atmos. Sci.*, **42,** 583–606.

——, and H. R. Pruppacher, 1988: A theoretical study of the wet removal of atmospheric pollutants—Part III: The uptake, redistribution, and deposition of $(NH_4)2\ SO_4$ particles by a convective cloud; using a two-dimensional cloud dynamics model. *J. Atmos. Sci.*, **45,** 1857–1871.

Fouquart, Y., B. Bonnel, G. Brogniez, A. Cerf, M. Chaoui, L. Smith and J. C. Vanhoutte, 1984: Size distribution and optical properties of Saharan aerosols during ECLATS. *Aerosols and their Climatic Effects,* H. E. Gerber and A. Deepak, Eds., A. Deepak Publishing, 35 pp.

Hänel, G., 1976: The properties of atmospheric aerosol particles as functions of the relative humidity at thermodynamic equilibrium with the surrounding moist air. *Adv. Geophys.*, **19,** 73–188.

Hoppel, W. A., J. W. Fitzgerald and R. E. Larson, 1985: Aerosol size distributions in air masses advecting off the east coast of the United States. *J. Geophys. Res.*, **90,** 2365–2379.

Jaenicke, R., 1984: Physical aspects of the atmospheric aerosol. *Aerosols and their Climatic Effects,* H. E. Gerber and A. Deepak, Eds., A. Deepak Publishing, 7 pp.

Junge, C. E., 1963: *Air Chemistry and Radioactivity.* Academic Press, 382 pp.

King, M. D., 1982: Sensitivity of constrained linear inversions to the selection of Lagrange multiplier. *J. Atmos. Sci.*, **39,** 1356–1369.

King, M. D., D. M. Byrne, B. M. Herman and J. A. Reagan, 1978: Aerosol size distributions obtained by inversion of spectral optical depth measurements. *J. Atmos. Sci.*, **35,** 2153–2167.

Ku, H. H., 1966: Notes on the use of propagation of error formulas. *J. Res. of Nat. Bureau. Stds. Engg and Instrument,* **70C,** 263–273.

Leckner, B., 1978: The spectral distribution of solar radiation at the earth's surface—elements of a model. *Sol. Energy,* **20,** 143–150.

Mészáros, E., 1981: *Atmospheric Chemistry Fundamental Aspects.* Elsevier, 91 pp.

Meyer, S. L., 1975: *Data Analysis for Scientists and Engineers.* Wiley, 39 pp.

Moorthy, K. K., P. R. Nair and B. V. Krishna Murthy, 1989: Multiwavelength solar radiometer network and features of aerosol spectral optical depth at Trivandrum. *Ind. J. Radio Space Phys.*, **18,** 194–201.

Parameswaran, K., and B. V. Krishna Murthy, 1990: Altitude profiles of tropospheric water vapor at low latitudes. *J. Appl. Meteor.*, **29,** 665–679.

——, K. O. Rose, M. Satyanarayana and B. V. Krishna Murthy, 1989: Method of analysis and preliminary results of atmospheric lidar observations at Trivandrum. *Ind. J. Radio Space Phys.*, **18,** 202–209.

Phillips, D. L., 1962: A technique for the numerical solution of certain integral equations of the first kind. *J. Assoc. Comput. Mach.*, **9,** 84–97.

Prodi, F., G. Santachiara and F. Oliosi, 1983: Characterization of aerosols in marine environments (Mediterranean, Red Sea, and Indian Ocean). *J. Geophys. Res.*, **88,** 10 957–10 968.

Prospero, J. M., R. J. Charlson, B. Mohnen, R. Jaenicke, A. C. Delany, J. Moyers, W. Zoller and K. Rahn, 1983: The atmospheric aerosol system: an overview. *Rev. Geophys. Space Phys.*, **21,** 1607–1629.

Quenzel, H., 1970: Determination of size distribution of atmospheric aerosol particles from spectral solar radiation measurements. *J. Geophys. Res.*, **75,** 2915–2921.

Rao, Y. P., 1976: Southwest monsoon. *Meteor. Monogr. Synoptic Meteorology,* No. 1,

Shaw, G. E., J. A. Reagan and B. M. Herman, 1973: Investigations of atmospheric extinction using direct solar radiation measurements made with a multiple wavelength radiometer. *J. Appl. Meteor.*, **12,** 374–380.

Shettle, E. P., and R. W. Fenn, 1979: Models for the aerosols of the lower atmosphere and the effects of humidity variation on their optical properties. AFGL-TR-079-0214,

Suzuki, T., and S. Tsunogai, 1988: Daily variation of aerosols of marine and continental origin in the surface air over a small island Okushiri in the Japan sea. *Tellus,* **40B,** 42–49.

Tomasi, C., 1979: Nonselective absorption by atmospheric water vapor at visible and near infrared wavelengths. *Quart. J. Roy. Meteor. Soc.*, **105,** 1027–1040.

Twomey, S., 1963: On the numerical solution of Fredholm integral equations of the first kind by the inversion of the linear system produced by quadrature. *J. Assoc. Comput. Mach.*, **10,** 97–101.

Whitby, K. T., 1978: The physical characteristics of sulfur aerosols. *Atmos. Environ.*, **12,** 135–159.